JOURNAL OF MATERIALS SCIENCE 31 (1996) 1779–1788

Microscopic aspects of polymer–metal epitaxy

K. D. JANDT*
Cornell University, Department of Materials Science and Engineering, Bard Hall, Ithaca, NY 14853-1501, USA

M. BUHK, J. PETERMANN
Universität Dortmund, Fachbereich Chemietechnik, Lehrstuhl für Werkstoffkunde, Emil-Figge-Straße 66, D-44221 Dortmund, Germany

The textured oriented overgrowth (epitaxy) of certain metals evaporated on to substrates consisting of highly oriented ultra-thin thermoplastic polymer films has been known for a few years. However, the origin of the observed epitaxy was not clear: the formation of a chemical interface layer, classic epitaxy or graphoepitaxy (artificial epitaxy) all seemed to be possible explanations for the observed orientations. We have used the complementary methods of transmission electron microscopy (TEM) and scanning force microscopy (SFM) to investigate aspects of the polymer–metal epitaxy. Our investigations show that the bulk morphologies of polymer substrates determine their surface topographic properties. Highly oriented surface steps serve as suitable locations for an oriented growth of the evaporated metals. The results of the investigations suggest artificial epitaxy (graphoepitaxy) as an effective orientation mechanism for the oriented metallic growth on polymer substrates.

1. Introduction

Controlled crystal-growth processes hold one of today's key positions in technological applications and basic research. Specifically, epitaxial growth phenomena such as homoepitaxy (A on A) [1] and heteroepitaxy (A on B) [2], are subjected to significant scientific and commercial interest, for example in the field of nanotechnologies.

In the area of heteroepitaxy, the crystallographic oriented overgrowth of certain metals, such as tin, indium, bismuth, and tellurium on to uniaxially oriented semi-crystalline ultra-thin polymer films such as polyethylene (PE), polypropylene (PP), polybutene-1 (PB-1), and syndiotactic polystyrene (sPS) has been known for nearly a decade [3, 4]. Applications of these composites are in the field of optical storage media [5] or anisotropic electric conductive films [6], because the polymer–metal epitaxy offers an economical and effective way to produce highly oriented metal layers with the desired physical properties for these applications.

However, the character of the polymer–metal epitaxy needs to be investigated in more detail, because the mechanism of the orientation is unclear. First, those experiments will focus on the various interactions between the metallic adsorbate and the polymer substrate surface. So far, graphoepitaxy [7], i.e. adsorbate orientation induced by nucleation on to oriented topographic features of the substrate, the formation of a chemical layer, for example consisting of metal–methyl groups building up the polymer–metal interface [8], or classic epitaxy, i.e. lattice matching [9], have been proposed as orientation mechanisms for the polymer–metal epitaxy.

For the investigation of a feasible graphoepitaxial influence on the ordered growth of metals on polymer substrates, it is necessary to study both the surface topography of the polymeric substrates before and after metal evaporation, and to characterize the specific growth behaviour of the metallic adsorbates. This task may be fulfilled with the transmission electron microscope (TEM) and the scanning force microscope (SFM) because both provide high-resolution images in real space. Here, we present the results of the microscopic investigations and discuss in how far the potential orientation models mentioned above fit the experimental reality.

2. Experimental procedure

The oriented semi-crystalline polymer substrates were prepared according to the method of Petermann and Gohil [10]: the polymer granulate (PE, PP, PB-1 or sPS) was dissolved in xylene (~ wt/wt 0.4 %). Some droplets of this solution were then deposited on a smooth surface of a glass slide where the solution was dispersed uniformly. By heating the glass slide to a temperature well above the crystallization temperature of the polymer in use, the solvent evaporated. From the resulting polymer melt a highly oriented

* Author to whom all correspondence should be addressed. E-mail: jandt@msc.cornell.edu

022–2461

ultra-thin film (thickness $\approx 0.1\ \mu m$) was drawn by a motor-driven cylinder ($v_x \approx 7\ cm\ s^{-1}$).

The samples then were prepared in two different ways. For TEM investigations, the films were cut into 3 mm × 3 mm pieces and mounted on copper grids. The films were fixed on highly oriented pyrolytic graphite (HOPG) or mica for scanning force microscopic (SFM) investigations.

The metals were evaporated on the ultra-thin polymer films in a Balzers™ BAE 080 evaporation chamber at a pressure of $\sim 5 \times 10^{-3}$ Pa. Deposition on to substrates was made at a temperature ranging between 293 K and 403 K. Metallic films were deposited to a thickness ranging from 0.5–25 nm at a deposition rate from 0.01–0.5 $nm\ s^{-1}$, monitored with a quartz crystal oscillating microbalance.

The polymer films were shadowed with platinum or platinum–iridium for the TEM investigations of the surface topographic features. The measurement of shadow length of surface topographic features of the substrates as a function of shadowing angle allows the measurement of surface step heights of about 1 nm or more. TEM investigations were performed on a Philips 400 T operated at 100 keV and a Jeol 2000-FX operated at 200 keV.

The SFM investigations of the pure samples surfaces were performed with a Nanoscope III from Digital Instruments. The images were recorded by mapping the vertical displacement of the nanoprobe as a function of its horizontal position. The function relating vertical displacement to intensity (the look up table) in these experiments is a linear grey-scale. Hence the contrast represents the relative height of the surface (white represents peaks, dark represents valleys).

The cantilevers used were supplied by the microscope manufacturer, and had a nominal force constant of 0.06 $N\ m^{-1}$. The forces applied with the SFM tip were $\leqslant 10^{-9}$ N. The imaging force was adjusted to just above the pull-off point of the cantilever as soon as possible after the first contact in order to reduce the applied force to the minimum possible for stable imaging. From time to time it was checked that the set point was stable and still at the same location of the force curve. No filtering was applied to the feedback signal or the images. All structures shown in the SFM images were reproducible independent of scanning frequency, scanning direction and x–y range.

3. Results and discussion

3.1. Surface morphology of the polymer substrates

Transmission electron microscopic investigations indicate that the bulk of the polymer substrates produced by the technique described above consist of crystalline and amorphous regions (semicrystalline polymer films) [10]. The morphology and the size of crystalline areas depend on the different types of polymers used, as well as on the processing parameters (e.g. film-drawing velocity, hot-plate temperature) [10, 11]. In general, three different crystalline bulk morphologies of the substrates can occur: needle crystals (consisting of extended chains), lamellar crystals (folded-chain crystals) or a combination of both (so-called shish-kebab crystals).

Figs 1 and 2 show transmission electron micrographs of platinum-shadowed polymer substrate surfaces of polyethylene and polybutene-1 respectively. As deducible from the electron diffraction patterns inserted in Figs 1 and 2, the crystalline polymer surface planes of all polymer substrates considered here are $\{h\,k\,0\}$ planes having only the [0 0 1] direction, the direction of the molecular orientation, in common. This is known as fibre texture.

Fig. 1 shows that the crystalline parts of the PE substrate consist of stacked lamellar crystals of a thickness of a few tens of nanometres. The amorphous parts between the lamellar crystals originating

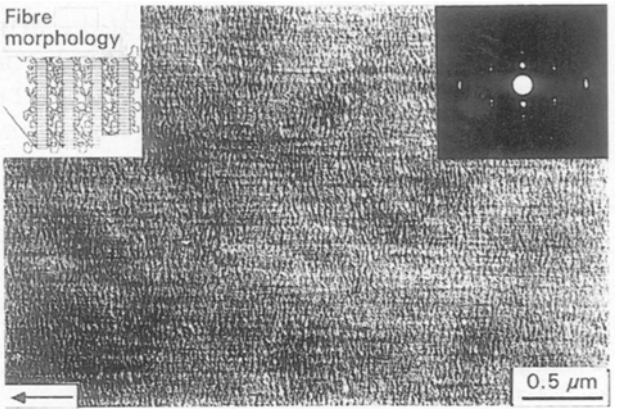

Figure 1 Transmission electron micrograph of a platinum shadowed PE substrate surface. The arrow in the lower left corner indicates the direction of the molecular orientation of the substrate. An electron diffraction pattern and a sketch showing the morphology of the semi-crystalline polymer are inserted in the upper right and left corners, respectively. The image shows two types of surface elevations: lamellae (dark) running vertically in the image (step height 1–5 nm) and process-induced steps (step height 5–20 nm) elongated parallel to the drawing direction of the substrate (arrow). The arrangement of steps in two directions perpendicular to each other leads to a quasi four-fold symmetry of the surface.

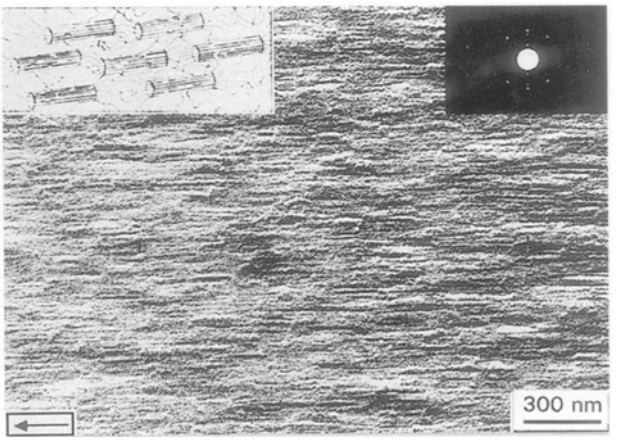

Figure 2 Transmission electron micrograph of a platinum shadowed PB-1 substrate surface. The arrow in the lower left corner indicates the direction of the molecular orientation of the substrate. An electron diffraction pattern and a sketch showing the morphology of the semi-crystalline polymer are inserted in the upper right and left corners, respectively. The image shows needle-like structures arranged parallel to the drawing direction of the substrate protruding from the surface for a few nanometres. The PB-1 surface exhibits a quasi two-fold symmetry relief.

from chain ends and chain foldings, as well as from less-ordered polymer chains, show about the same thickness as do the lamellae. Owing to a phase contribution to the image contrast, the lamellae in Fig. 1 appear as dark bands running approximately perpendicular to the drawing direction, whereas the amorphous parts appear brighter. A detailed analysis of the micrograph shows that the lamellae protrude from the amorphous substrate regions for 1–5 nm. Because the outstanding side faces of the lamellae consist of chain folds and chain ends, the side-edges of the steps show an amorphous character.

Additional to the steps generated by the lamellae, steps running approximately parallel to the drawing direction are visible in Fig. 1. It is believed that these steps are caused by non-uniform forces applied in the drawing direction during film preparation, leading to biaxial deformation and stress states of the polymer film (process-induced surface steps). These steps have an average length of 10 μm and a diameter between 10 and 100 nm. Their average height was measured to range between 5 and 20 nm.

From earlier TEM investigations it is known that the crystalline areas of the PB-1 substrate shown in Fig. 2 are built up of needle like crystals aligned parallel to the drawing direction of the polymer film [12]. The needle crystals are embedded in an amorphous highly oriented polymer matrix. The platinum-shadowed surface shown in Fig. 2 exhibits needle-like structures which are aligned parallel to the drawing direction of the substrate. These structures protrude from the surface for 2–5 nm. Their dimensions range from a few nanometres to some micrometres in length while, their diameter is found to be 30–60 nm.

Like the PE substrates the PB-1 substrate surfaces show evidence for process-induced surface steps. In the case of similar dimensions, an exact differentiation between needle-like structures and surface structures induced by the drawing process is not always possible.

For PP substrates which show a needle crystalline morphology, mostly similar results compared to those obtained from PB-1 have been found. Deviating from the PB-1 results, the steps heights of needle-like structures of PP were found to be 1–3 nm, which indicates that the PP substrates are, in general, flatter than PB-1 substrates.

A comparison between a transmission electron micrograph of a shadowed PE substrate surface and a related SFM image of a neat (unshadowed) PE substrate surface is shown in Fig. 3. The images show an arrangement of close-packed lamellar crystals. For both the TEM and the SFM part of the image the dimensions of surface topographic features of the substrate have been found to be similar. The SFM image shows more morphological details, such as interlocking and branching of individual lamellae, because the surface features are not modified or covered by platinum. Further SFM investigations showed structural modulations along the long axes of the lamellae and evidence for slip traces and/or growth terraces on top of the lamellae [13]. High-resolution SFM imaging of the crystalline surfaces of the lamellae showed evidence that the $\{1\,0\,0\}_{PE}$ planes are the preferred surface

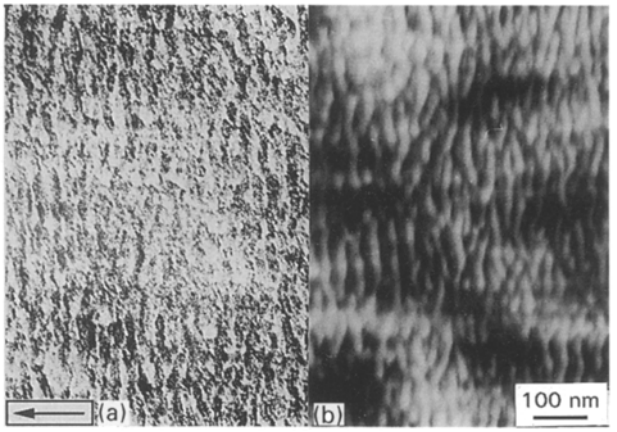

Figure 3(a) Transmission electron micrograph of a platinum shadowed PE substrate surface in comparison with (b) an SFM image of a neat (unshadowed) PE substrate surface. The values for lamellar thickness, step height of the outstanding lamellae, etc., were found to be similar with both techniques. Nevertheless, the SFM image shows more morphological details of the substrate, such as lamellar interlocking and branching of individual lamellae. The arrow in the lower left corner indicates the direction of molecular orientation.

planes [13–16]. At the amorphous, folded edges of the lamellae, evidence for sharp chain folds with adjacent re-entry of the PE chains has been found [15, 16].

The fact that the crystalline parts of the film protrude from the film surface was explained by a combination of film-processing and crystal-growth effects [13]: during the drawing process of the film, the molecules in the middle of the film are more stretched than the molecules at the surfaces. This is due to a different relaxation behaviour of the film surface compared to its centre. The result of this process may be a higher density of chain folds at the surfaces. It is assumed that during the growth process of the crystals, both parts of a chain related to a fold, are diffusing into the same growing crystals [13]. Some extended chains in the centre of the film are unable to follow this motion, because they are embedded in two adjacent crystals. The result of these processes leads to zones of less polymeric material (the lower amorphous areas). In the case of perfectly oriented chains in the centre of the film, extended chain crystals, as backbones for the lamellar overgrowth, can occur.

SFM imaging of a neat PB-1 substrate surface revealed structures as shown in Fig. 4a [17]. The image shows four needle crystals arranged parallel to each other. All crystals are oriented approximately parallel to the drawing direction. Their length was measured to be several hundred nanometres, whereas their diameter was found to be 20–55 nm. Additionally, the needle crystals protrude from the surface. The height from the region between the crystals and the top of the crystals was measured to be 0.5–4 nm (local values). These values are in good agreement with the values obtained from the transmission electron micrographs of shadowed PB-1 substrate surfaces (see above). In the upper part of the centre needle crystal, crystalline branching is visible. Between the needle crystals, elongated grooves (lower surface areas) oriented parallel to the needle axes are visible. The surfaces of the needle

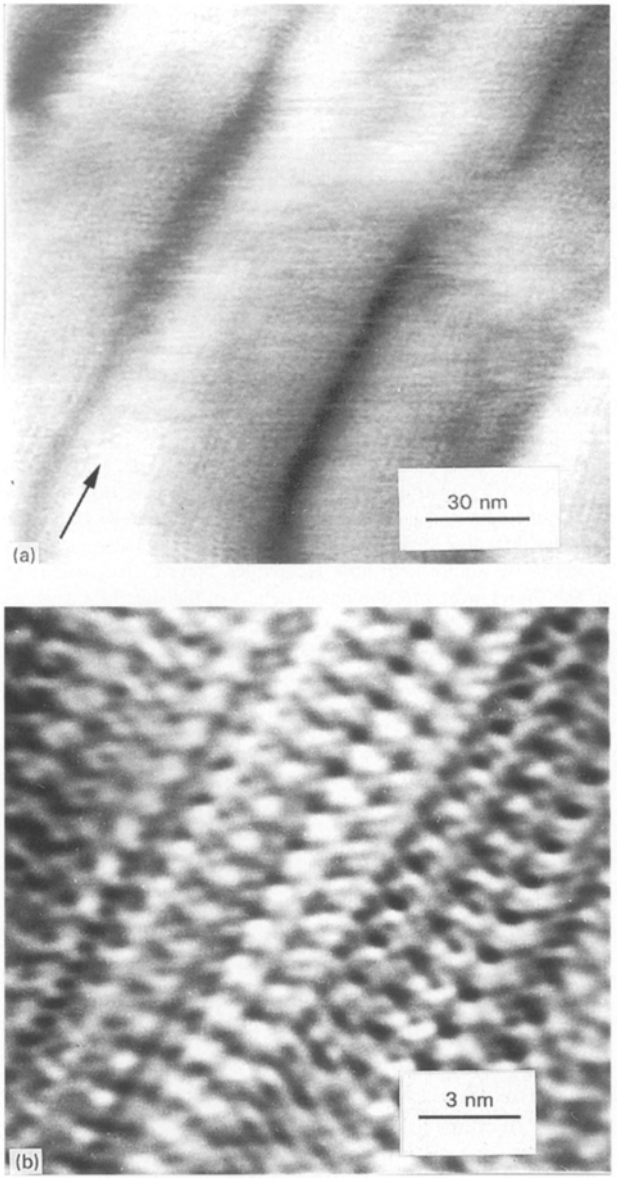

Figure 4(a) SFM image of a PB-1 substrate showing four needle crystals arranged parallel to each other diagonally crossing the scan area. The arrow in the lower left corner indicates the direction of the molecular orientation. Note the fine structure of lines arranged parallel to the long axes of the needle crystals and the molecular orientation. (b) At a higher magnification, the needle crystal surfaces show individual PB-1 macromolecules (helices). Along the chain directions of the macromolecules, a repeat (pitch height) of 0.7 $\pm$0.1 nm was obtained.

crystals exhibit a molecular fine structure arranged parallel to the long axes of the needle crystals and the drawing direction.

By increasing the magnification further to a molecular scale, images like Fig. 4b were obtained [17]. The image shows structures similar to PB-1 macromolecules (helices) with a repeat (pitch height) of 0.7 $\pm$0.1 nm along the molecular backbone, but other larger values (0.9 $\pm$0.1 nm) were also obtained at other areas of the needle crystals. In many cases the repeat values vary from the bulk value obtained from X-ray diffraction data of 0.65 nm [18]. Structures shown in Fig. 4b were reproducible independent of scanning frequency, scanning direction and x–y range.

Although the determination of the pitch height (intramolecular distance) from images like Fig. 4b is straightforward, it is more difficult to obtain values for the intermolecular distances in planes parallel to the surface, due to the complex and detailed surface structure. It is assumed that linear uninterrupted structures oriented parallel to the drawing direction in Fig. 4b are the backbones of PB-1 macromolecules. The structures between these backbones may originate from interlocking ethyl side groups of the PB-1 macromolecules. A typical value obtained for the intermolecular distance in planes parallel to the surface is 1.2 $\pm$0.3 nm but larger values (e.g. 1.5 nm) were also obtained. This value may be compared with the intermolecular distance in the bulk of a PB-1 crystal: e.g. in the $\{1\,0\,0\}_{\mathrm{PB-1}}$ planes the PB-1 helices are arranged in alternating distances of 0.59 and 1.18 nm. It should be emphasized here, that the difference in the observed intermolecular packing observed with the SFM compared to the bulk value may result from a non-crystalline and loose-molecular packing at surfaces compared to the bulk.

Further evidence for the observation that the outermost surfaces of the needle crystals are more loosely packed arises from the observation of the (upper limits of) diameter of the needle crystals in the SFM investigations (55 nm) and the TEM investigations of the shadowed PB-1 substrates (60 nm), because the diameters of needle crystals normally do not exceed 50 nm. In the case of isotactic polystyrene, earlier TEM dark-field images revealed a diameter of 31.3 $\pm$3 nm for the needle crystals, whereas SFM measurements showed evidence for a 60% larger diameter of the same substrate [19]. The larger observed diameters of the needle crystals in the case of our surface investigations may be explained by the fact that TEM dark-field investigations image the crystalline part of the needles only, whereas by TEM surface shadowing and SFM the whole needle morphology, including its surface, is imaged. Hill *et al.* proposed that the needles consist of a crystalline core and a transitional zone of highly ordered molecules (hair dressing model) [20, 21]. In the transitional zone, no long-range lateral order exists and hence, it is not accessible to dark-field TEM.

As in the case of the lamellar crystals, the fact that the needle crystals protrude from the surface may be explained by a diffusion of macromolecules from the amorphous matrix towards the growing needle crystals. This may result in an (topographically lower) amorphous zone of less polymeric materials and in the observed topographic relief.

3.2. Growth of metals on the polymer surfaces

Fig. 5 shows a transmission electron micrograph of an PB-1 substrate evaporated with 1 nm Sn at 303 K. After the tin deposition, the substrate surface was shadowed with platinum to allow the study of the surface topography. As deducible from the micrograph, most of the tin crystallites have grown in surface grooves oriented parallel to the drawing direction of the film. As shown in the last section, these

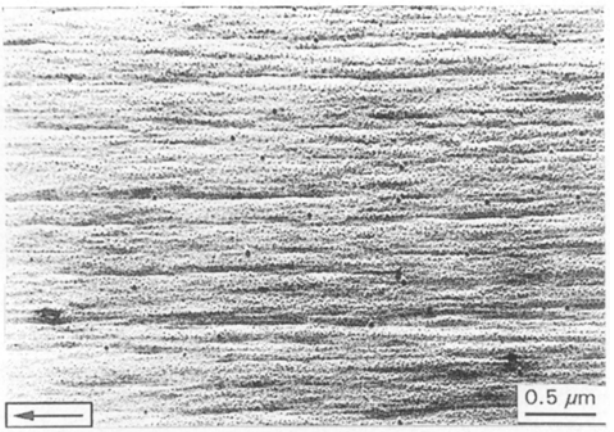

Figure 5 Transmission electron micrograph of a PB-1 substrate evaporated with 1 nm Sn at 303 K. After the tin deposition the substrate was shadowed with platinum for surface investigations. The tin crystallites are visible as dark spots. Most of them have grown at surface steps of the substrate (decoration of the lower edges of the steps).

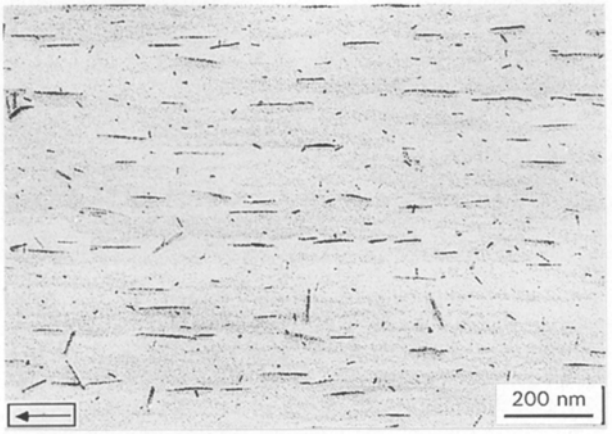

Figure 6 Transmission electron micrograph of a PP substrate evaporated with 2 nm Te at 363 K. After the tellurium deposition the substrate was shadowed with platinum for surface investigations. The tellurium crystallites are visible as needles aligned parallel to the drawing direction of the substrate. Most of them have grown at surface steps of the substrate (decoration of the lower edges of the steps).

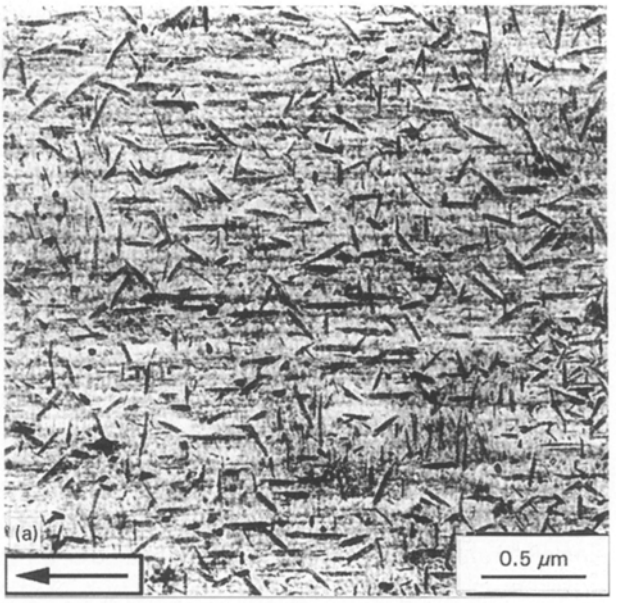

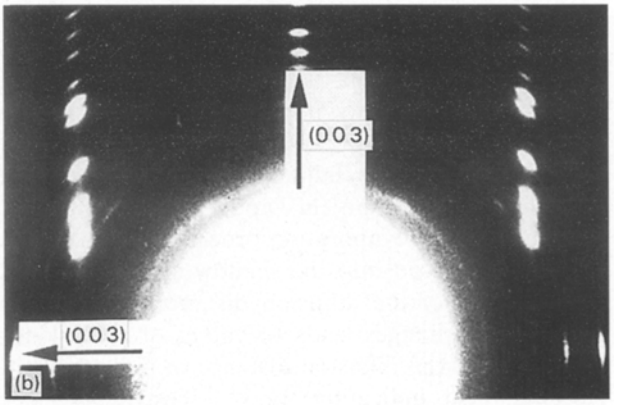

Figure 7(a) Transmission electron micrograph of a PE substrate evaporated with 4 nm Te at 363 K. After the tellurium deposition, the substrate was shadowed with platinum for surface investigations. In the micrograph two main morphological orientations of the Te crystallites perpendicular and parallel to the molecular orientation are visible. These tellurium crystallites decorate the lower edges of the lamellae and the process-induced surface steps, respectively. The two preferred morphological orientations reflect the two preferred crystallographic orientations $[0\,0\,1]_{Te} \parallel [0\,0\,1]_{PE}$, $(h\,k\,0)_{Te} \parallel (h\,k\,0)_{PE}$ and $[0\,0\,1]_{Te} \perp [0\,0\,1]_{PE}$, $(h\,k\,0)_{Te} \parallel (h\,k\,0)_{PE}$ deducible from the electron diffraction pattern in (b). Note the two $(0\,0\,3)_{Te}$ reflexes perpendicular to each other. In the electron diffraction pattern, the $[0\,0\,1]_{PE}$ direction is horizontal.

grooves are, in general, located between the needle crystalline parts of the substrate or between process-induced surface steps. In the first case the tin crystallites are also in contact with one or more side faces of the needle crystals adjacent to the grooves (see Fig. 12); in the latter case, the tin crystallites are in contact with the process-induced steps. This decoration effect occurs owing to the fact that for energetic reasons, substrate surface steps are the preferred locations for nucleation and growth of adsorbate crystallites (see for example [22, 23]).

The surface-step decoration effect of the metallic adsorbates on PP substrates in the case of overgrown tellurium crystallites is shown in Fig. 6. In this case, the rod-like Te crystallites are grown in the grooves between the surface steps.

In the case of lamellar substrate morphologies (e.g. PE), two different locations of surface decoration of the metallic adsorbates were found. As shown in the transmission electron micrograph in Fig. 7a most of the tellurium crystallites decorate the process-induced surface steps oriented parallel to the drawing direction of the substrate, as well as the lower edges of the lamellae running perpendicular to the drawing direction of the substrate (see Fig. 11). In both cases the rod-like tellurium crystallites are oriented parallel to the respective step direction (morphological orientation). Because the rod axis of each tellurium crystallite coincide with the crystallographic *c*-direction of the crystallite, we would expect two different preferred orientations of the tellurium crystallites. The related electron diffraction pattern of a similar unshadowed sample is shown in Fig. 7b. As deducible from the electron diffraction pattern, two preferred orientations of the overgrowing tellurium crystallites occur: $[0\,0\,1]_{Te} \parallel [0\,0\,1]_{polymer}$, $(h\,k\,0)_{Te} \parallel (h\,k\,0)_{polymer}$

and $[0\,0\,1]_{Te} \perp [0\,0\,1]_{polymer}$, $(h\,k\,0)_{Te} \parallel (h\,k\,0)_{polymer}$. The fact that the electron diffraction spot of the latter orientation is less intense can be explained by a noticeable tilt between the step edges of the lamellae and the average substrate plane, leading to a tilt in crystalline growth at these steps. The steps oriented parallel to the drawing direction of the film seem to be more or less parallel to the average film plane. Two preferred orientations of tin perpendicular to each other ($[1\,0\,0]_{Sn} \parallel [0\,0\,1]_{polymer}$ and $[1\,0\,0]_{Sn} \perp [0\,0\,1]_{polymer}$) have been observed earlier on substrates also with lamellar morphology [24].

Another characteristic of the oriented overgrowth of metals on polymer substrates is the surface mobility of the metal particles during and after the metal deposition process. This can be deduced from TEM images similar to that shown in Fig. 8. The transmission electron micrograph shows a surface area of a PE substrate evaporated with tin. The direction of the metal vapour beam was tilted 70° to the surface. In the upper right part of the micrograph, a dust particle is visible. The left part of the micrograph shows tin crystallites growing on the surface, whereas most of the PE surface area shown in this micrograph is in the vapour shadow area of the dust particle. In this area only very small tin crystallites decorating the lamellae are visible. Because no tin vapour reaches this area during the metal evaporation process, these particles have been diffused into the shadow area. A detailed measurement of the diffusion distances in this and similar TEM images leads to values of several micrometres for the diffusion distance of individual tin particles, also indicating weak adhesive (van der Waals) forces between the substrates and the adsorbates. A low adhesion and a high surface mobility of the metal deposits during and after the metal deposition process have also been confirmed by SFM investigations [14] and by measurements of the conductivity of the metal films [6].

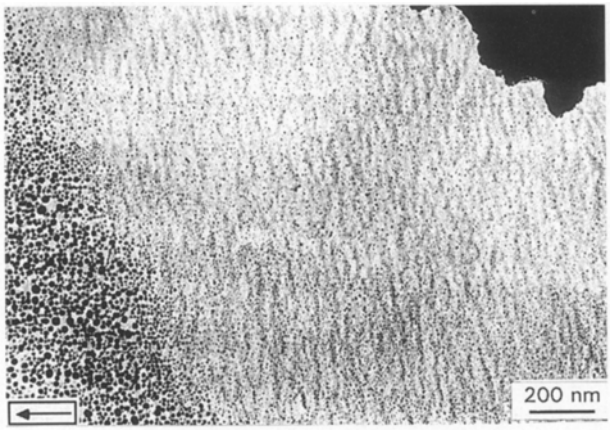

Figure 8 Transmission electron micrograph showing a surface area of a PE substrate evaporated with tin. The direction of the metal vapour beam was tilted 70° to the surface normal. In the upper right part of the micrograph, a dust particle is visible. The left part of the micrograph shows tin crystallites growing on the surface, whereas most of the PE surface area shown in this micrograph is in the vapour shadow area of the dust particle. In this area only very small tin crystallites decorating the lamellae are visible. Because no tin vapour reaches this area during the metal evaporation process, these particles have been diffused into the shadow area.

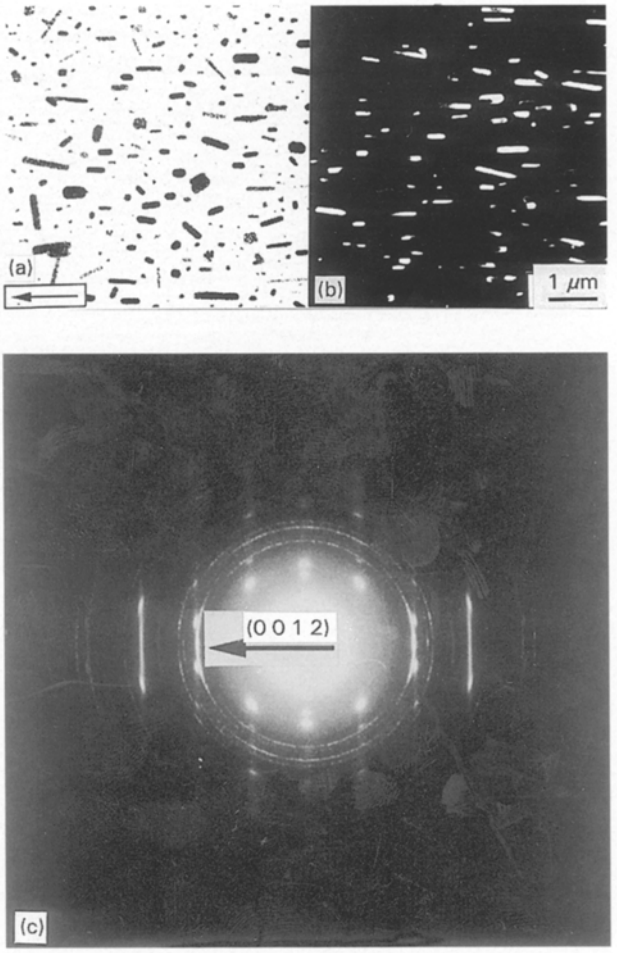

Figure 9(a–c) Transmission electron micrographs showing a PB-1 substrate evaporated with 20 nm Tl at 303 K. The whiskers visible in the image consist of Tl_2O and show a preferred morphological orientation with their elongated axes parallel to the drawing direction of the substrate. The TEM dark-field micrograph (b) was done with the (0 0 1 2) reflex of the hexagonal Tl_2O. As deducible from the electron diffraction pattern of the sample shown in (c) the preferred crystallographic orientation is $[0\,0\,1]_{Tl_2O} \parallel [0\,0\,1]_{PB-1}$ and $(h\,k\,0)_{Tl_2O} \parallel (h\,k\,0)_{PB-1}$.

When evaporating 20 nm thallium to PB-1 substrates cylindrical morphologies of the deposits as shown in Fig. 9a–c were obtained. The TEM images show that most of the cylinders were grown parallel to the drawing direction. The crystallographic orientation of the cyclinders is deducible from both the TEM dark-field micrograph shown in Fig. 9b and the electron diffraction pattern shown in Fig. 9c. A detailed analysis of this electron diffraction pattern showed that the cylinders consist not of thallium but its oxide Tl_2O. As far as we are aware this is the first observation of a metal oxide showing an epitaxial effect on highly oriented semicrystalline polymer substrates. The preferred orientation was found to be $[0\,0\,1]_{Tl_2O} \parallel [0\,0\,1]_{PB-1}$. When evaporating 15 nm or less thallium on a PB-1 substrate and subsequently shadowing the substrate surface, TEM images as shown in Fig. 10a were obtained. The images show individual Tl_2O cyclinders embedded in elongated surface grooves as well as elliptical Tl_2O islands on the surface. Because more of these islands were found at low nominal Tl_2O thicknesses, it is assumed that they are precursors of the cylindrical Tl_2O

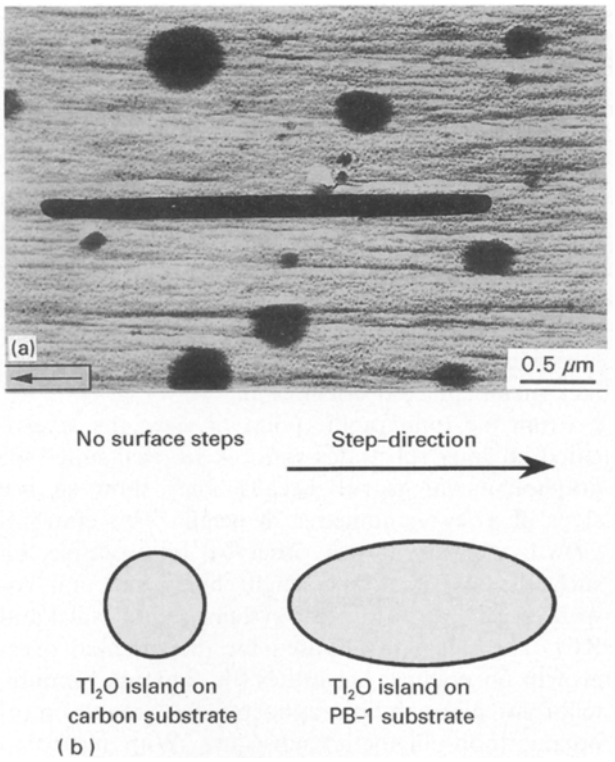

Figure 10(a) Transmission electron micrograph of a PB-1 substrate evaporated with 15 nm Tl at 333 K. After the thallium evaporation the substrate was shadowed with platinum. In this micrograph two different morphologies (elliptical Tl_2O islands and a Tl_2O cylinder) are shown. The Tl_2O cylinder grew along an elongated surface groove. Note that the shape of some of the edges of the elliptical islands is influenced by the surface topography. (b) A comparison of the circular Tl_2O islands morphology found on amorphous carbon substrates (left) and the elliptical Tl_2O island morphology found on PB-1 substrates (right). It is supposed that the elliptical shape of the Tl_2O islands is caused by anisotropic diffusion of Tl_2O on the step-rich PB-1 surface.

crystallites. On amorphous carbon substrates these islands were found to be of a circular morphology. Therefore, it is assumed that their shape is influenced by an anisotropic surface diffusion caused by the anisotropic surface structure of the PB-1 surface as shown in Fig. 10b. This assumption is supported by the observation that on lamellar substrates (PE) which have surface steps in two perpendicular directions, no epitaxial effect of the Tl_2O was observed.

3.3. Model for the growth mechanism

Earlier X-ray photoelectron spectroscopy (XPS) measurements indicated the presence of a chemical layer at the metal–polymer interface [8]. It was supposed that the interface layer may consist of metal organic compounds or oxygen. Under certain conditions, cross-linking of PE chains at the substrate surface after metal evaporation was observed [25, 26]. Chemical reactions at the interface seem to be possible if the surfaces of the polymers are reactive, if the metal adsorbates have special chemical affinities to parts of the polymer substrates, if the adsorbates have a sufficient kinetic energy to provide chemical reactions on the substrate surface, or if the energy released during the metal condensation process is sufficient for breaking C–H or C–C bonds. PS, PB-1, PP, and PE consist of saturated hydrocarbon chains which, similar to paraffin, have a small tendency for chemical reactions [27]. In the absence of ionizing radiation and strong oxidizing agents, PS, PB-1, PP, and PE are some of the most resistant materials to chemical reactions due to their chemical inertness.

The boiling point for tin at 10^{-3} Pa (pressure during evaporation) is 1155 K [28]. From the laws of the kinetic theory of gases, we deduce that about 10^{15} tin particles/cm^{2}s hit the polymer surface at this temperature. As indicated by the reaction rate in Table I only nine of them have a kinetic energy larger than 3.4 eV (Maxwell distribution), the bond energy of a C–C bond of polymer. For all other investigated metals the number of particles having sufficient energy for C–C bond breaking is even less (see Table I) and therefore negligible.

Another source for the supply of the energy necessary for bond breaking is the heat released during the metal condensation process, ΔH_c, values which are shown in Table II [28]. For the metals under consideration, tin has the highest value of ΔH_c

TABLE II Heat of condensation, ΔH_c, of the metals showing an oriented overgrowth on polymer substrates. The ΔH_c values of the elements shown in the table are smaller than the C–H binding energy ($E_B \approx 415\,kJ\,mol^{-1}$) and the C–C binding energy ($E_B \approx 331\,kJ\,mol^{-1}$) indicating that ΔH_c is insufficient for inducing chemical reactions

Element	Heat of condensation, ΔH_c (kJ mol^{-1})
Sn	295.80
Te	52.55
Bi	104.80
In	231.50
Tl	164.10

TABLE I The kinetic and energetic data of the metals showing an oriented overgrowth on polymer substrates. The right column shows the reaction rate of the metal particles. In the case of tin, only nine tin atoms/cm^2 s have a kinetic energy $\geqslant$ 3.4 eV. These atoms may react with the polymer substrate, e.g. via bond breaking

Particles in the gas phase	Boiling temperature T_s at 10^{-3} Pa (K)	Hitting rate, Z_w, at 10^{-3} Pa (cm^{-2}s^{-1})	Average kinetic energy, E_m (eV)	Fraction of particles with $E_{kin} \geqslant 3.4$ eV, N (3.4 eV, ∞)/N_0	Reaction rate, R (Particles/cm^2 s)
Sn	1155	9.2×10^{14}	0.150	9.6×10^{-15}	9
Te_2	534	9.3×10^{14}	0.069	7.9×10^{-32}	7×10^{-17}
Bi	745	8.6×10^{14}	0.096	8.2×10^{-23}	7×10^{-7}
In	943	1.0×10^{15}	0.122	4.9×10^{-18}	5×10^{-3}
Tl	685	9.1×10^{14}	0.089	8.3×10^{-25}	8×10^{-10}

(295.80 kJ mol^{-1}) . A comparison of ΔH_c with the bond energies of the C–C bonds of the hydrocarbon chains ($E_B \approx 331$ kJ mol^{-1}) shows that ΔH_c is lower than the bond energy, indicating that ΔH_c is not sufficient to induce bond breaking at the polymer surfaces. The bond energy for the C–H bonds of the hydrocarbon chains is even higher ($E_B \approx 415$ kJ mol^{-1}). In conclusion, a chemical reaction at the considered epitaxial polymer–metal interfaces is unlikely.

A required condition for a classic epitaxy between the lattices of substrates and adsorbates is a lattice mismatch (deviation of lattice constants between substrate and adsorbate along a direction) between both of $\delta \leqslant 15\%$ [2]. The mismatch δ (%) is defined as $\delta = 100\,(b - a)/a$, where a and b are the lattice parameters of substrate and adsorbate, receptively. Considering a classic epitaxial orientation mechanism for polymer–metal epitaxial growth, the cases of a geometric fitting (lattice matching) between the lattices of the polymeric substrates and the metallic adsorbates are shown in Table III. In some cases, a matching can occur when one lattice parameter of substrate or adsorbate fits to twice a lattice parameter of adsorbate or substrate. These cases are indicated by, for example, $2c_{PE} \parallel a_{Sn}$.

Matchings of the periodic arrangements of polymer chains at surface planes were examined additionally. These cases are important for monoclinic PP crystals, because the crystallographic a and b directions of these crystals are not arranged normal to their crystallographic c-axes (chain direction). Therefore, the shortest distance between two polymer chains, for example in the $\{0\,1\,0\}_{PP}$ plane, is $d_{PP} = a_{PP} \cos(99°20' - 90°) \approx 0.657$ nm. The results of these matching calculations are shown in Table IV. As deducible from the tables, only a few of the experimentally observed polymer–metal systems fulfil the condition of a small mismatch, as for example in the case of $\{0\,1\,0\}_{PP} \parallel \{0\,1\,0\}_{In}$. For most of the experimentally observed orientations, the condition of lattice matching is not fulfilled, indicating that classic epitaxy via lattice matching is not a general explanation of polymer–metal epitaxial orientation.

From the topographic point of view, the investigated polymer substrates surfaces are well suited for graphoepitaxial growth because they show surface steps of a few nanometres in height. This epitaxial growth mechanism was observed, for example, on surface steps of atomic height by Osaka and coworkers [23, 30–34] for the systems tin on NaCl and KCl. The same metals used for the oriented overgrowth on polymer substrates (tin, indium, bismuth, tellurium) also exhibit graphoepitaxial growth on inorganic (non-polymeric) substrates. With regard to the step orientations, their graphoepitaxial orientations on such substrates are similar to those observed on stepped polymer surfaces.

Prerequisites for an oriented overgrowth of the metals on to polymer substrates seem to be a low melting point and a distinct anisotropic crystal lattice of the metals because, for example, gold does not show

TABLE III The table shows all cases found for a lattice matching beween lattice parameters of the polymer substrates and the adsorbates in parallel planes

Substrate contact plane	Lattice constants in contact plane (nm)	Adsorbate contact plane	Lattice constants in contact plane (nm)	Cases of matching in parallel directions substrate–adsorbate	Mismatch δ (%)
PE	$c = 0.255$	Sn	$a = 0.583$	$2c_{PE} \parallel a_{Sn}$	14.3
$\{0\,1\,0\}$	$a = 0.742$	$\{1\,0\,0\}$	$c = 0.318$	$a_{PE} \parallel 2c_{Sn}$	− 14.2
PE	$c = 0.255$	Bi	$b = 0.455$	$2c_{PE} \parallel b_{Bi}$	− 10.6
$\{0\,1\,0\}$	$a = 0.742$	$\{0\,0\,0\,1\}$	$\lvert\langle 1\,1\,0\rangle\rvert = 0.788$	$a_{PE} \parallel \lvert\langle 1\,1\,0\rangle\rvert_{Bi}$	6.2
PE	$c = 0.255$	Bi	$b = 0.455$	$2c_{PE} \parallel b_{Bi}$	− 10.6
$\{1\,1\,0\}$	$\lvert\langle 1\,1\,0\rangle\rvert = 0.891$	$\{0\,0\,0\,1\}$	$\lvert\langle 1\,1\,0\rangle\rvert = 0.788$	$\lvert\langle 1\,1\,0\rangle\rvert_{PE} \parallel \lvert\langle 1\,1\,0\rangle\rvert_{Bi}$	− 11.6
PB − 1	$c = 0.650$	Te	$c = 0.593$	$c_{PB-1} \parallel c_{Te}$	− 8.8
$\{1\,0\,0\}$	$a = 1.770$	$\{1\,1\,0\}$	$\lvert\langle \bar{1}\,1\,0\rangle\rvert = 0.771$	$a_{PB-1} \parallel 2\lvert\langle 1\,1\,0\rangle\rvert_{Te}$	− 12.9

TABLE IV Matching between regular chain distances of the polymer substrates and metal crystals

Substrate contact plane	Lattice constants in contact plane (nm)	Adsorbate contact plane	Lattice constants in contact plane (nm)	Cases of matching in parallel directions substrate–adsorbate	Mismatch δ (%)
PP	$c = 0.650$	Sn	$a = 0.583$	$c_{PP} \parallel a_{Sn}$	− 10.3
$\{0\,1\,0\}$	$d_{PP} \approx 0.657$	$\{1\,0\,0\}$	$c = 0.318$	$d_{PP} \parallel 2c_{Sn}$	− 3.1
PP	$c = 0.650$	In	$\lvert\langle 1\,0\,1\rangle\rvert = 0.675$	$c_{PP} \parallel \lvert\langle 1\,0\,1\rangle\rvert_{In}$	3.8
$\{0\,1\,0\}$	$d_{PP} \approx 0.657$	$\{0\,1\,0\}$	$\lvert\langle \bar{1}\,0\,1\rangle\rvert = 0.675$	$d_{PP} \parallel \lvert\langle \bar{1}\,0\,1\rangle\rvert_{In}$	2.7
PB − 1	$c = 0.650$	Sn	$a = 0.583$	$c_{PB-1} \parallel a_{Sn}$	− 10.3
$\{1\,1\,0\}$	$d_{PB-1} \approx 1.02$	$\{0\,0\,1\}$	$b = 0.583$	$d_{PB-1} \parallel 2b_{Sn}$	14.3
PB − 1	$c = 0.650$	Te	$c = 0.593$	$c_{PB-1} \parallel c_{Te}$	− 8.8
$\{1\,1\,0\}$	$d_{PB-1} \approx 1.02$	$\{1\,0\,0\}$	$a = 0.445$	$d_{PB-1} \parallel 2a_{Te}$	− 12.7

any orientational relationship to the polymer substrates. Furthermore, the results suggest an important influence of the surface mobility of the metallic adsorbates during and after the evaporation process, to establish low-energy metal planes in contact with the polymer substrates.

The experimental results suggest an orientation mechanism shown schematically in Fig. 11 in the case of lamellar polymer substrates and in Fig. 12 in the case of fibrillar polymer substrates. For lamellar polymer substrates, the metal crystallites decorate the surface steps which are caused by the protrusion of the crystalline parts of the substrate from the rest of the surface. Because the edges of these steps consist of amorphous surface regions (chain foldings, chain ends), the overgrowing metal crystallites are not in contact with crystalline parts of the substrate, having a long-range order of polymer chains. As deducible from the orientations of the metals, all considered metals have planes of low surface energy in contact with the substrate. Therefore, the orientation is caused by the step directions of the substrate and a minimization of the surface free energy of the absorbates.

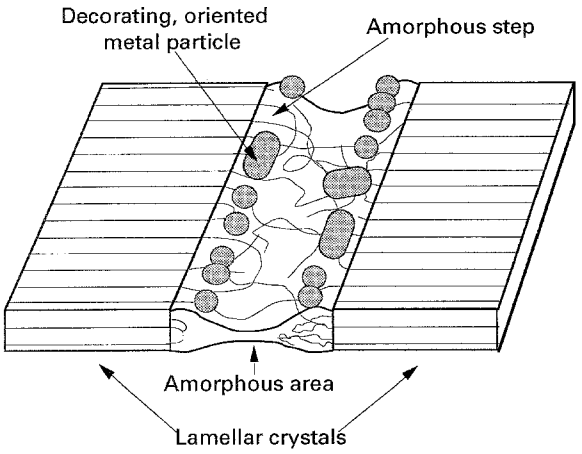

Figure 11 Schematic sketch demonstrating how metal crystallites orient on a lamellar polymer substrate. The lamellae protrude from the amorphous regions of the surface. Owing to the folded character of the lamellar side faces, the decorating metal crystallites are in contact with amorphous surface regions. The orientation may be caused by surface energy minimization of the metal crystallites and their alignment respective to the step direction.

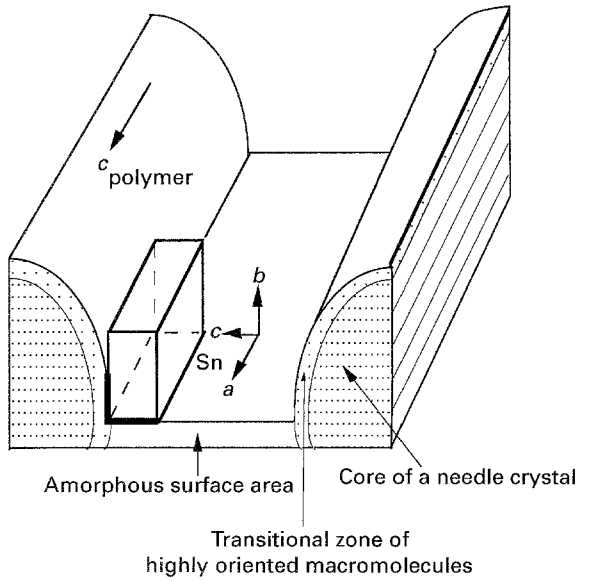

Figure 12 Schematic sketch demonstrating how metal crystallites orient on a fibrillar polymer substrate. In this sketch, a tin crystallite was chosen as an example for the metallic overgrowth. The low-index contact plane faces the amorphous polymer material. Tin crystallites align with $[1\,0\,0]_{Sn} \parallel [c]_{polymer}$. An orientation is established via minimization of the surface free energy of the tin crystallite in contact with the amorphous polymer steps. The crystallographic *a*-axis of the tin crystallite then orients with respect to the step direction.

In the case of fibrillar morphology, the metal crystallites decorate the surface steps caused by needle crystals protruding from the surface. Because the metal crystallites are in contact with highly oriented but non-crystalline polymeric material, no crystallographic information can be transferred from the polymer substrate to the overgrowing metal crystallites.

Owing to the occurrence of macromolecular chain foldings of the PE lamella, the surface steps of PE substrates exhibit an amorphous character [14]. From earlier TEM investigations it was proposed that the needle crystals of fibrillar PB-1 substrates consist of a crystalline core and a transitional (amorphous) zone of highly oriented molecules (hair dressing model) [20, 21]. Under these conditions, the metal crystallites growing at the edges of polymeric surface steps (decoration) are in contact with polymeric material having no long-range order (see Fig. 12). Therefore, the orientation of the metal particles on to polymer substrate surface steps seems to be a result of minimization of surface free energy of the particles in contact with the step edges.

Very little is known about the initial stages of the polymer–metal epitaxial growth. Nevertheless, it should be noted that the so-called Volmer–Weber or island growth mode seems to be the most likely. The reason is that the considered polymer substrates are chemically inert materials. Therefore, any deposits (especially the metals considered above) should adhere weakly to such substrates. Earlier SFM investigations of metal evaporated polymer substrates confirm this assumption [14].

4. Conclusions

1. When deposited on to $\{h\,k\,0\}$ planes of uniaxially oriented semi-crystalline polymer substrates, several metals tend to grow epitaxially. It is found that the semi-crystalline nature of the polymeric substrates leads to nanostructured polymer surfaces. The observed surface steps of a few nanometers in height exhibit an amorphous character. In the case of lamellar substrate morphology, the edges of these steps consist of folded polymer chains or chain ends. For fibrillar substrate morphologies the contact faces of the steps consist of highly oriented but non-crystalline polymeric material. Additionally, all substrates exhibit process-induced surface steps oriented along the drawing direction of the substrates.

2. The majority of the overgrowing metal crystallites at the polymeric surfaces decorate the lower edges of the surface steps. Because lamellar polymer substrates exhibit surface steps in both directions, parallel and perpendicular to the drawing direction of the

substrate, two preferred orientations of overgrowing metals perpendicular to each other (for example, for tellurium and tin) were observed. The orientation of the metals seems to be caused by surface energy minimization of the crystallites at highly oriented polymer steps (graphoepitaxy).

3. The new epitaxial system Tl_2O on PB-1 was observed. This is the first observation of a metal-oxide growing crystallographically oriented on highly oriented polymer substrates.

4. Lattice matching (classic epitaxy) is not a general explanation for the oriented overgrowth of the metals because only a few cases of geometric matching between the metal crystallites and the polymer substrates were found. The other observed orientations cannot be explained with lattice matching because of larger mismatchings.

5. The formation of a chemical interface layer between the polymer substrates and the metals seems to be unlikely, because the polymer substrates are relatively inert. The kinetic (hitting) energy of the metals during the evaporation process and the heat of condensation of the metals supply insufficient energy for significant polymer bond breaking.

Acknowledgements

The authors acknowledge the financial support of the Volkswagen Foundation and the Deutscher Akademischer Austauschdienst. J. Petermann acknowledges the financial support of the Fond der Chemischen Industrie (FCI).

References

1. H. BENEKING, "Halbleiter-Technologie" (Teubner, Stuttgart, 1991) pp. 88–149.
2. J. W. MATTHEWS, "Epitaxial Growth" (Academic Press, New York, London, Toronto, Sydney, San Francisco, 1975).
3. J. PETERMANN and G. BROZA, *J. Mater. Sci.* **22** (1987) 1108.
4. J. M. SCHULTZ and S. K. PENEVA, *J. Polym. Sci. Part B Polym. Phys.* **25** (1987) 185.
5. J. PETERMANN, A. WERNER and H. HIBST, Patent DE 3608267 A1 (1986).
6. T. HOFFMANN, Ph D thesis, Technische Universität Hamburg-Harburg, Germany (1993).
7. M. W. GEIS, D. C. FLANDERS and H. I. SMITH, *Appl. Phys. Lett.* **35** (1979) 71.
8. M. JUNG, U. BASTON, P. STEINER and J. PETERMANN, *J. Mater. Sci.* **26** (1991) 5467.
9. J. M. SCHULTZ and S. K. PENEVA, "RHEED Investigation of Thin Tin Films on Polypropylene", APS-meeting Bulletin, Las Vegas (American Physica Society, 1986) 511.
10. J. PETERMANN and R. M. GOHIL, *J. Mater. Sci* **14** (1979) 2260.
11. B. WUNDERLICH "Macromolecular Physics", Vol. 1, "Crystal Structure, Morphology, Defects" (Academic Press, New York, London, Toronto, Sydney, San Francisco, 1973).
12. K. WENDEROTH, A. KARBACH and J. PETERMANN, *Coll. Polym. Sci.* **263** (1985) 301.
13. K. D. JANDT, M. BUHK, M. J. MILES and J. PETERMANN, *Polymer* **35** (1994) 2458.
14. K. D. JANDT, "Untersuchungen zur Polymer-Metall-Epitaxie in Computersimulation und Experiment", Fortschr.-Ber. VDI Reihe 5 no. 302 (VDI, Düsseldorf, 1993).
15. L. M. ENG, H. FUCHS, K. D. JANDT and J. PETERMANN, *Helv. Phys. Acta* **65** (1992) 870.
16. L. M. ENG, K. D. JANDT, H. FUCHS and J. PETERMANN, *Appl. Phys.*, **A59** (1994) 145.
17. K. D. JANDT, T. McMASTER, M. J. MILES, and J. PETERMANN, *Macromolecules* **26** (1993) 6552.
18. G. NATTA, P. CORRADINI and I. W. BASSI, *Nuovo Cimento Suppl.* **15** (1960) 52.
19. K. D. JANDT, L. M. ENG, J. PETERMANN and H. FUCHS, *Polymer* **24** (1992) 5331.
20. M. J. HILL, P. J. BARHAM and A. KELLER, *Polym. Sci.* **258** (1980) 1023.
21. M. J. HILL and A. KELLER, *Coll. Polym. Sci.* **259** (1981) 335.
22. J. H. MAGILL, In "Treatise on Material Science and Technology", edited by J. M. Schultz, Vol. 10, Part A (Academic Press, New York, 1977) p. 142.
23. T. OSAKA, T. KAWANA, T. NOIJIAMA and K. HEINEMANN, *J. Cryst. Growth* **61** (1983) 509.
24. J. R. REFFNER, E. L. THOMAS and J. PETERMANN, unpublished data (1991).
25. S. L. VOGEL and H. SCHONHORN, *J. Appl. Phys.* **23** (1979) 495.
26. G. SCHERER, Dissertation D386, Kaiserslautern University, Germany (1985).
27. B. DOLEZEL, "Die Beständigkeit von Kunststoffen und Gummi" (Carl Hanser, München, Wien, 1978) p. 392.
28. W. ESPE, "Werkstoffkunde der Hochvakuumtechnik", Bd. 1, "Metalle und metallisch leitende Werkstoffe" (VEB Deutscher verlag der Wissenschaften, Berlin, 1960) 879 f.
29. "Table of Periodic Properties of the Elements", (Sargent-Welch Scientific Company, Skokie, Il, 1980).
30. T. OSAKA, T. KAWANA, T. NOIJIAMA, K. HEINEMANN, *J. Cryst. Growth* **61** (1983) 509.
31. T. OSAKA, Y. KASUKABE and H. NAKAMURA, *ibid.* **69** (1984) 149.
32. T. OSAKA and Y. KASUKABE, *ibid.* **73** (1985) 10.
33. Y. KASUKABE and T. OSAKA, *Thin Solid Films* **146** (1987) 175.
34. T. OSAKA and Y. KASUKABE, in "Proceedings of the First Topical Meeting on Crystal Growth Mechanisms" (Izu Nagaoka, 1989) p. 87.
35. P.-M. KLEWS, R. ANTON and M. HARSDORFF, *J. Cryst. Growth* **71** (1985) 491.
36. *Idem, J. Vac. Sci. Technol. A* **5** (1987) 1931.

Received 4 August 1994
and accepted 8 September 1995